

Tropospheric circulation during the early twentieth century Arctic warming

Martin Wegmann^{1,2} · Stefan Brönnimann^{1,2} · Gilbert P. Compo^{3,4}

Received: 12 October 2015 / Accepted: 30 May 2016
© Springer-Verlag Berlin Heidelberg 2016

Abstract The early twentieth century Arctic warming (ETCAW) between 1920 and 1940 is an exceptional feature of climate variability in the last century. Its warming rate was only recently matched by recent warming in the region. Unlike recent warming largely attributable to anthropogenic radiative forcing, atmospheric warming during the ETCAW was strongest in the mid-troposphere and is believed to be triggered by an exceptional case of natural climate variability. Nevertheless, ultimate mechanisms and causes for the ETCAW are still under discussion. Here we use state of the art multi-member global circulation models, reanalysis and reconstruction datasets to investigate the internal atmospheric dynamics of the ETCAW. We investigate the role of boreal winter mid-tropospheric heat transport and circulation in providing the energy for the large scale warming. Analyzing sensible heat flux components and regional differences, climate models are not able to reproduce the heat flux evolution found in reanalysis and reconstruction datasets. These datasets show an increase of

stationary eddy heat flux and a decrease of transient eddy heat flux during the ETCAW. Moreover, tropospheric circulation analysis reveals the important role of both the Atlantic and the Pacific sectors in the convergence of southerly air masses into the Arctic during the warming event. Subsequently, it is suggested that the internal dynamics of the atmosphere played a major role in the formation in the ETCAW.

Keywords Arctic climate · Arctic warming · Circulation · Reanalysis · Reconstructions · Troposphere · Climate change · Heat flux

1 Introduction

Global mean temperature increased by ca. 0.5 °C between 1910 and 1945 (Hansen et al. 2010), a phenomenon known as “early twentieth century warming”. Although anthropogenic forcing contributed (Bindoff et al. 2013), unusual internal variability is normally held responsible (Delworth and Knutson 2000), which some have related to increasing North Atlantic sea-surface temperatures (Schlesinger and Ramankutty 1994). Recent work also has pointed to possible tropical Pacific influences (Thompson et al. 2015).

The early twentieth century warming was characterized by concurrent regional warming episodes (Brönnimann 2009), the most pronounced of which was strong warming of the Arctic from the late 1910s to the 1940s, here called “early twentieth century Arctic warming” (ETCAW). Palaeoclimatic data suggest that, until the beginning of the twenty-first century, the ETCAW was unique in magnitude and rate for at least the last 1500 years in the Arctic domain (Kaufman et al. 2009; Pages 2K Consortium 2013; Opel et al. 2013). Understanding the ETCAW and its links

Electronic supplementary material The online version of this article (doi:10.1007/s00382-016-3212-6) contains supplementary material, which is available to authorized users.

✉ Martin Wegmann
martin.wegmann@giub.unibe.ch

- ¹ Oeschger Centre for Climate Change Research, University of Bern, Bern, Switzerland
- ² Institute of Geography, University of Bern, Hallerstrasse 12, 3012 Bern, Switzerland
- ³ Cooperative Institute for Research in Environmental Sciences, University of Colorado, Boulder, CO, USA
- ⁴ Physical Sciences Division, NOAA Earth System Research Laboratory, R/PSD1 325 Broadway, Boulder, CO 80305, USA

to global climate and the oceans might therefore unravel important mechanisms in the climate system. One objective of this paper is to gain more insight into triggering mechanisms for the ETCAW.

Though noticed and studied by contemporary scientists (Birkeland 1930; Scherhag 1939; Wagner 1940), the ETCAW again became a prominent research topic in the 1980s and 1990s in the context of global change [see Grant et al. (2009) and Wood and Overland (2010) for a discussion of ETCAW studies]. Research has been conducted with sparse direct observations at the surface (Bekryaev et al. 2010), or in the upper air (Grant et al. 2009), climate model experiments, and gridded reconstructions (Brönnimann et al. 2012). The respective analysis of those datasets underlined the exceptional nature of this event (Wood and Overland 2010; Opel et al. 2013). More recently, long reanalysis data sets have become available (e.g., Compo et al. 2011; Poli et al. 2016) that allow analyzing atmospheric circulation in more detail. In our paper we make use of these new data sets and compare them with model and reconstruction data.

Compared to the present Arctic warming, the ETCAW was mainly confined to the European Atlantic sector (Scherhag 1939; Bengtsson et al. 2004; Wood and Overland 2010; Bekryaev et al. 2010). In the vertical, recent maxima of temperature anomalies are mostly found at the surface whereas the maximum warming of the ETCAW was located in the mid troposphere (Grant et al. 2009; Brönnimann et al. 2012). This suggests a different role of atmospheric circulation for the two warming events (IPCC 2013).

Therefore, a variety of possible warming mechanisms are suggested in the literature. It was found that during the ETCAW southerly winds into the Arctic domain prevailed. This meridional windflow was strongest over the Atlantic and transported warmer air masses northwards (Wood and Overland 2010). Pressure anomalies show an increase over the Eurasian sector of the Arctic landmasses and a negative anomaly over Greenland and the Labrador Sea (Grant et al. 2009). Furthermore, Grant et al. (2009) argue that this circulation pattern supported the aerosol transport from Central Europe to the Arctic. There is evidence for an increase of sulphate aerosols in the European Arctic from a Svalbard ice core. These aerosols might have led to a positive feedback of the warming during winter.

Several studies point out a high probability of increased winter sea surface temperatures (SSTs) and reduced winter sea ice cover north of 60°N during the ETCAW, comparable to the situation at the end of the twentieth century (Hanssen-Bauer and Førland 1998; Johannessen et al. 2004; Bengtsson et al. 2004; Semenov and Latif 2012). Unfortunately, sea ice cover observations are sparse before 1940 and model studies can only point towards tendencies.

However, it remains an open question whether the oceanic signals preceded atmospheric changes or vice versa.

Finally, internally (Polyakov et al. 2003) and externally (Overpeck et al. 1997) forced low frequency cycles have been linked to the onset and peak of the ETCAW. External forcing in the form of greenhouse gases is most likely not the dominant factor to the ETCAW. Fyfe et al. (2013) found that in model experiments the warming between 1900 and 1939 can be better explained by natural forcings than by greenhouse gas changes. However, other anthropogenic forcings such as aerosols may have contributed.

Beitsch et al. (2014) investigated a 3000 year Earth System model integration and analyzed the climatic conditions of 26 Arctic warming events within this simulation, utilizing superposed epoch analysis. They found a triggering ocean warming signal that induces atmospheric changes triggered by reduced sea ice over the Barents–Kara seas. Additionally, they found a strong increase of stationary atmospheric energy transport into the Arctic during the warming event, whereas transient and mean meridional energy transports decrease. The authors conclude that ETCAW-like events can be caused by internal (decadal) variability of the ocean and atmosphere system.

Therefore, the ETCAW exemplifies the importance of yearly and decadal internal variability on Arctic climate. Although much research effort was spent to understand the links and influences of and on the ETCAW, the ultimate cause is still under discussion. The comparison of the ETCAW to the recent warming period grants a chance to deepen the knowledge about the drivers of Arctic climate and recent Arctic amplification of global warming (Wood and Overland 2010).

Here, we use state of the art, multi-member global circulation models (GCMs), climate reanalysis and upper air reconstructions to examine the tropospheric dynamics during the ETCAW. We extend the analysis of Wood and Overland (2010) and Beitsch et al. (2014) concerning an intensified meridional circulation over the Atlantic Arctic and focus on mid-tropospheric heat transport. For this we include two recently published reanalysis datasets, ERA-20C and the Twentieth Century Reanalysis Version 2c (20CRv2c), and assess the variability seen in these new datasets over Arctic regions. We define an index to investigate Arctic circulation regimes that can amplify energy transport into the Arctic domain. This allows us to compare the mechanism of atmospheric Arctic warming over time.

This article is structured as follows. Section 2 gives an overview of the various datasets analyzed. Section 3 describes the methods used. Section 4 presents the results for tropospheric circulation and transportation patterns. After discussing the results in Sect. 5, conclusions are drawn in Sect. 6.

2 Data

In this study we use six different datasets to assess Arctic warming and its associated tropospheric dynamics. As listed below, they consist of two global circulation models, three reanalysis datasets, and one statistically reconstructed upper-air dataset.

2.1 Model data

To assess the relative impact of internal and external variability, we compare reconstructions and reanalysis datasets with two different sets of ensemble model experiments. The European Centre for Medium-Range Weather Forecasts (ECMWF) integrated an ensemble of ten Integrated Forecast System (IFS) atmospheric simulations for the years 1899–2009 at a horizontal resolution of T_L159 with 91 vertical levels reaching from the surface up to 1 Pa, which is known as the experimental ERA-20cm version (ERA20CM). Specified sea–ice concentration and sea surface temperature boundary conditions come from an ensemble of realizations (HadISST.2.0.0.0), where the variability in these realizations is based on the uncertainties in the observational sources used. The radiation scheme follows exactly the CMIP5 protocol, including aerosols, ozone and greenhouse gases (Hersbach et al. 2015).

The second general circulation model (GCM) dataset consists of a 30 member ECHAM5.4 atmosphere model (Roeckner et al. 2006) simulations spanning from 1599 to 2005 (Bhend et al. 2012; CCC400). It was integrated at a triangular spectral truncation of T63 and with 31 levels in the vertical up to 10 hPa. The model was forced with monthly mean sea surface temperatures (SSTs) based on an annual reconstruction of (Mann et al. 2009). Sea ice according to the longterm HadISST1.1 climatology is used before 1870 and HadISST1.1 reconstructed sea ice thereafter (Rayner et al. 2003). Volcanic radiative forcing is computed online as in Jungclaus et al. (2010) based on reconstructions by Crowley et al. (2008), consisting of aerosol optical depth (AOD) at 0.55 μm and effective particle radii in four latitude bands [see Wegmann et al. (2014) for details]. Furthermore, the model was forced by observed greenhouse gases (Yoshimori et al. 2010), tropospheric aerosols (Koch et al. 1999), total solar irradiance (Lean 2000), and land surface conditions (Pongratz et al. 2008).

2.2 Reanalyses

The NOAA-CIRES Twentieth Century Reanalysis V2 (20CRv2) dataset allows retrospective 4-dimensional analysis of climate and weather between 1871 and 2012 (Compo et al. 2011). It was achieved by assimilating

surface observations of synoptic pressure using an Ensemble Kalman Filter assimilation system. Prescribed boundary conditions are HadISST1.1 (Rayner et al. 2003) monthly SST and sea ice cover fields as well as specified time-varying incoming solar radiation and concentrations of CO₂ and volcanic aerosols. Here we use the ensemble mean of the 56 ensemble members with a spatial resolution of T62 and a 6-hourly temporal resolution. Unfortunately, 20CRv2 is affected by a misspecification of sea ice, which affects the atmosphere (Brönnimann et al. 2012).

The NOAA-CIRES Twentieth Century Reanalysis Version 2c (20CRv2c) uses the same model and assimilation system as 20CRv2 but with new sea ice boundary conditions from the COBE-SST2 (Hirahara et al. 2014), new pentad Simple Ocean Data Assimilation with sparse input (SODAsi.2, Giese et al. 2016) sea surface temperature fields, and additional observations from ISPD version 3.2.9 (Cram et al. 2015). SODAsi.2 was forced with winds and bulk fluxes from 20CRv2. SODAsi.2c is generated by tapering SODAsi.2 at 60°N/S to COBE-SST2 SSTs, which makes the Arctic sea ice and SSTs consistent. For assimilated observational pressure data, 20CRv2c and ERA-20C have exactly the same pressure data input in the Northern Hemisphere.

The ERA-20C reanalysis (Poli et al. 2016) uses the IFS model in a 4-D Var system to assimilate observations of surface pressure and marine surface winds. It is a global atmospheric reanalysis for the period 1900–2010 with a 3-hourly temporal resolution and the same spatial and vertical resolution as ERA-20CM. It shares the same boundary conditions and CMIP5 radiative forcing with ERA-20CM, however for sea ice and SSTs HadISST2.1 is used.

2.3 Reconstructions

We use statistically reconstructed monthly temperature and geopotential height fields for the period 1880–1957 (Griesser et al. 2010) where the predictors are historical surface data from station observations (temperature), gridded sea-level pressure (SLP), and, after 1918, upper-air data (temperature, geopotential height (GPH) or pressure, and winds). Hemispheric GPH and temperature fields at six levels (850, 700, 500, 300, 200, 100 hPa) were used as predictands. This reconstruction is termed REC1. For analyzing the long term variation of anomaly fields, we merge this dataset with the equivalent fields in ERA40 (Uppala et al. 2005) to create a dataset which spans the continuous time period 1880–2002. It should be noted however, that ERA40 shows some issues for temperature in the free troposphere after the 1980s, affecting late twentieth century trends (Grant et al. 2008).

For annual near surface temperature over the Barents–Kara sea region, we averaged the Akademii Nauk ice cap

$\delta 18\text{O}$ record reconstructions from Opel et al. (2013), the Vardø and Arkhangelsk surface air temperatures (SATs) measurements (Brohan et al. 2006), Atlantic–Arctic boundary region measured SAT anomalies (Wood et al. 2010) and measured Arctic SAT anomalies (Polyakov et al. 2003) (for individual timeseries see supplementary Figure 1).

3 Analysis procedure

Here we investigate the Arctic temperature variations during the northern hemisphere cold season (DJF). Concerning the ETCAW, Bekryaev et al. (2010) found that boreal winter together with autumn showed the strongest warming signal. During boreal winter, temperature differences between polar and subpolar airmasses are strongest, and therefore northward heat transport is strongest. Overland and Turet (1994) reported that Northern Hemisphere poleward energy transport is maximized between 800 and 600 hPa. We therefore focus on the 700 hPa level as a surrogate for mid-tropospheric processes.

We compare all gridded datasets with regards to their Arctic winter temperature evolution during the twentieth century. For this, we area average the gridded datasets over a defined region in the Arctic domain. To analyze the role of tropospheric circulation in the ETCAW, we compute different components of northward heat transport at 700 hPa and 60°N in the GCM, reanalysis and reconstruction datasets. The zonal mean northward heat flux can be written as

$$\overline{vT} = \overline{v} \cdot \overline{T} + \overline{v^* \cdot T^*} + \overline{v' \cdot T'} \quad (1)$$

where v is meridional wind in m/s, T is air temperature in Kelvin, the overbar denotes the time (here monthly) mean, the brackets denote the zonal mean, the stars denotes the deviation from the zonal average, and the prime denotes the deviation from the time average. The first term on the right hand side describes the flux due to the time mean (here monthly) meridional circulation, followed by the flux due to stationary (time averaged) eddies and the flux due to transient eddies. Stationary eddies represent large-scale Rossby waves whereas transient eddies encompass cyclonic and anti-cyclonic disturbances in the flow (note that a separation is not strictly possible; we use 1 month as a threshold mainly for convenience, as this allows us to also look at monthly data sets). Since the REC1 dataset only offers monthly variables, we focus on the first two terms at the right hand side, which can be calculated for it. However, we extended the analysis of the three reanalysis datasets to the transient eddy flux as well. As will be shown later, reanalyses are inconsistent with respect to the mean meridional (first) term. The model data is not suited to compute the transient eddy term since the temporal resolution is too

low. Therefore this study focuses mainly on the stationary eddy contribution.

To gain more insight into the mechanisms of the stationary eddy transport, we define an index to display circulation regimes that transport airmasses in and out the Arctic domain over two key regions: the Atlantic sector (extension of Siberian high and Greenland low) and the Bering strait (Aleutian low and extension of Siberian high). These regions were the key action centers of the circulation configuration during the ETCAW as well as the key patterns of the second empirical orthogonal function in most datasets (not shown). A timeseries of this index should reveal periods of similar circulation conditions throughout the twentieth century. However, we find that the expression of the second EOF, often known as the Arctic Dipole if used for the Arctic Domain, depends largely on the nature of the datasets. The 3rd and 2nd EOF patterns might switch depending on the datasets, thus we introduce here this simplified, but stable index for investigating meridional circulation configurations.

We assume that during winter most of the heat is transported from the mild oceans to the Central Arctic. Therefore, we concentrate on the Pacific and Atlantic sectors. We selected regions as shown in Fig. 1 and calculated DJF anomalies of area-averaged geopotential height at 700 hPa for each of the four areas. Since the Atlantic connection to the Arctic is much wider, the corresponding boxes are

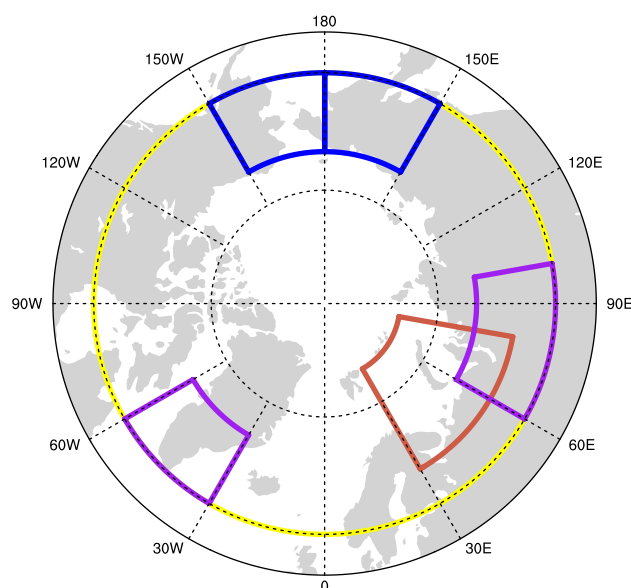


Fig. 1 Purple sectors showing regions for computing the Atlantic sector index ($60^\circ\text{--}70^\circ\text{N}$ $30^\circ\text{--}60^\circ\text{W}$ Greenland, $60^\circ\text{--}70^\circ\text{N}$ $60^\circ\text{--}100^\circ\text{E}$ Siberia), blue sectors showing regions for computing the Pacific sector index ($60^\circ\text{--}70^\circ\text{N}$ $150^\circ\text{--}180^\circ\text{W}$ Alaska, $60^\circ\text{--}70^\circ\text{N}$ $150^\circ\text{--}180^\circ\text{E}$ Far East). The yellow band indicates the 60°N latitude defined as Arctic boundary in this study. The red sector indicates the location of the Barents–Kara Sea region

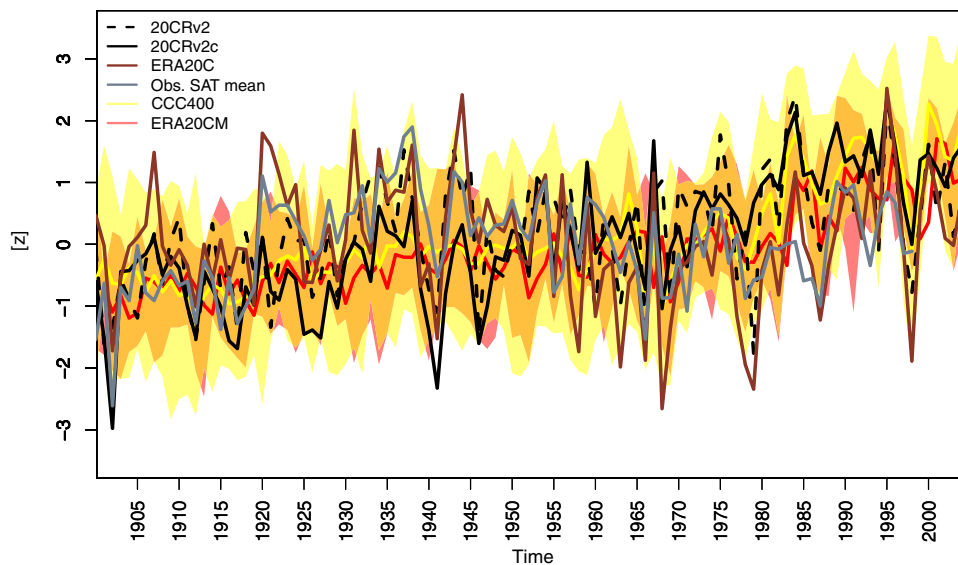


Fig. 2 Yearly mean 2 m temperature from 1900 to 2005 area-averaged for the Barents–Kara sea region (65° – 90° N, 30° – 90° E), in CCC400 (yellow transparent shading is spread of ensemble members), ERA20CM (red transparent shading is spread of ensemble

members), 20CRv2, 20CRv2c, and an index comprised of the mean of one SAT reconstruction and four station based SAT compilations (see Opel et al 2013). Time series are plotted as normalized deviations from the 1900 to 1998 mean

further away than for the Pacific case. Moving the Siberian box to the west, weakens the amplitude of the signal but the results are similar. With this setup, the strength of the Siberian high is captured as well. The reference period was set to the winters of 1971–2000. These values are then normalized by the total standard deviation of the anomaly time-series. Eventually, the index is computed as the difference between the values in the eastern region and the western region:

$$GPH\ INDEX = \overline{GPH}_E - \overline{GPH}_W \quad (2)$$

\overline{GPH} represents standardized monthly anomalies of geopotential height and the subscripts denote the eastern and the western area. For the ensemble datasets, the index was first calculated for each individual ensemble member and averaged thereafter.

A positive index corresponds to a high pressure situation in the east and a relatively lower pressure field in the west, which induces a northward flow into the Arctic.

4 Results

4.1 Arctic temperature evolution

Extraordinarily mild temperatures in the Arctic during the 1930s gave rise to the phrase “Early Twentieth Century Arctic Warming”. To assess the different datasets in regards to this important variable, we compare SAT from

reconstructions and observations with 2 m temperature from the gridded datasets. Figure 2 illustrates different timeseries of near SAT evolution in the Barents–Kara sea region (see Table S1 for correlations). A mean of reconstructed, station measured, and paleo datasets is used as an index for an observational estimate of the regional average. It shows positive anomalies between 1920 and 1940, with a first distinctive peak in 1920 and a second, stronger peak in 1937/1938. After three cold years (1940–1942), another peak occurred in 1943/1944. The individual series comprising the index show interesting variations in the timing and amplitude of the details of the ETCAW (Fig. S1). The large-scale area average from the reanalyses provides complementary estimates of the variability, with surprising similarities to the index. The reanalyses can be compared directly with each other and with the GCM simulations. Examining the reanalyses in detail, ERA20C has the largest standardized expression of the 1920 and 1944 peaks, whereas 20CRv2 has smaller amplitudes for 1920 and 1938 peaks. The comparison with both the index and ERA-20C is closer in 20CRv2c, which shows reduced amplitudes. We find that 20CRv2 shows very good agreement with the observational proxy in the first 20 years of the century, consistent with good global agreement (Compo et al. 2011). Overall, the 20CRv2c and ERA20C agree better with the observational index than the older 20CRv2 (Table S1).

The GCM data indicate that the ensemble of model realisations spans the variance of the reanalysis and

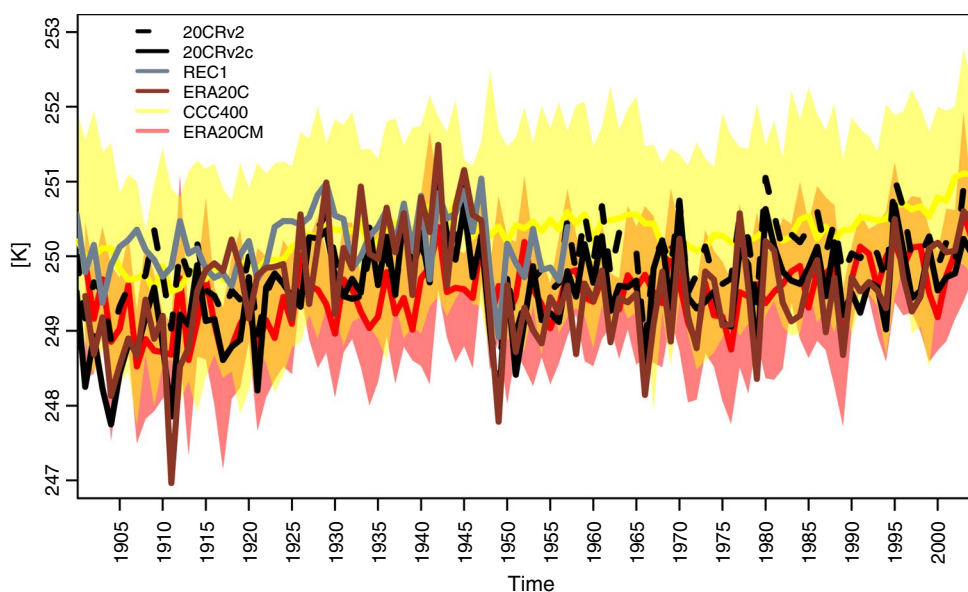


Fig. 3 DJF 700 hPa area average temperature 1900–2005 for the Arctic (60° – 90° N) from the models CCC400 (yellow transparent shading is spread of ensemble members) and ERA20CM (red trans-

parent shading is spread of ensemble members), as well as the reanalyses 20CRv2, 20CRv2c, ERA20C, and the reconstruction REC1

observational timeseries rather well. It is interesting to note that the ERA20C appears to be at the upper edge of the GCM values until ca. 1950, after which it resembles more the lower part of the distribution of the GCM ensemble. Towards the end of the twentieth century, 20CRv2 deviates away from the observational index and ERA20C, but is still well within the GCM range. The newer 20CRv2c decreases this deviation, probably from the improved specification of sea ice concentration.

The ERA20CM ensemble shows a smaller ensemble spread than CCC400, but both model ensemble means agree quite well with each other (See Table S1). The two periods with increasing temperatures (1900–1940 and 1980–2010) are visible in all datasets, although four timeseries represent an ensemble mean. Nevertheless, with the exception of ERA20C, all datasets underestimate the ETCAW and overestimate the Arctic near surface warming in the latter half of the twentieth century compared to the observational index. However, in general, all gridded datasets show surprisingly close resemblance in magnitude and tendency to the observational index.

Since this study focuses on the atmospheric circulation features of the ETCAW, a good representation of upper air warming is an important necessity of the used datasets. Figure 3 shows the DJF temperature timeseries for the area average of 60° – 90° N at 700 hPa for all atmospheric datasets being studied. ERA20CM and CCC400 show rising temperatures between 1910 and 1940, stable to cooling temperatures between 1940 and 1980, and a weak temperature increase after this until the start of the twenty-first

century. The ETCAW appears relatively warm in the model datasets, but appears to be split into peaks before and after 1935 in contrast to the earlier surface warming peak identified in ERA20C and the observational index. The temperature drop in the GCMs after 1940 could arise from the 1940 to 1942 El Niño event contained in the specified SSTs (Brönnimann et al. 2004). ERA20CM, on average, shows 1–2 K lower values than CCC400, which is a known feature of ERA20CM (Hersbach et al. 2015). Temperature maxima in the four reanalysis datasets appear around 1940, which is comparable to the surface timeseries.

All four observation-based datasets agree very well in magnitude and correlation (Table S2), staying within the variability of the models. It is worth mentioning that the reconstruction and reanalyses show a mid-tropospheric temperature signal during the ETCAW, which is unique in magnitude until the twenty-first century. Additionally, a sharp drop can be seen in the late 1940s in the reanalysed and reconstructed temperatures. Finally, the prominent Arctic warming signal at the end of the twentieth century is depicted by all atmospheric datasets with similar positive tendencies. In general, GCMs, reanalyses, and reconstructions values match well (see supplementary Tables 1–6). CCC400 compares better until the 1950s, after which ERA20CM is closer to reanalysed temperatures. This is probably due to different forcing input when compared to CCC400. Nevertheless, most of the time reconstructed and reanalyzed values are within the CCC400 ensemble variability. 20CRv2 and 20CRv2c agree very well over time, especially during the ETCAW. Generally, 20CRv2 tends

more towards the lower values of ERA20C in the first twenty and last 50 years of the century. We find that the 20CRv2c version improves the representation of upper tropospheric temperatures, surface/tropopause temperature gradient [see Brönnimann et al. (2012) for discussion of 20CRv2 performance] and the stretch out of the warming into the lower troposphere (see Supplementary Figures 2–4). Thus, the new sea ice data and added observations seem to improve the temperature signal at the surface. Generally, it is expected from all surface-input reanalysis datasets, that the skill decreases with altitude, especially so in the Arctic. These differences are lowest at mid-troposphere levels such as 700 or 500 hPa. Compared to the other reanalyses, reconstruction, and CCC400, an overall cold bias of ERA20C and ERA20CM at the 700 hPa level is found in the Arctic area average (Fig. S5). Examining the temporal variability, after 1946 a strong step function is seen in for 700 hPa temperature the reanalysis datasets. The magnitude of the jump seems to be partly a consequence of surface observation assimilation, since REC1 and the GCMs do not reproduce the amplitude. Including upper air data in the ERA20C assimilation scheme decreases the temperature drop compared to the original surface data assimilation, as suggested by an experimental ERA-pre-SAT reanalysis using upper-air data, see Hersbach et al., manuscript in preparation (supplementary Figure 5).

4.2 Zonal heat transport at 700 hPa

Since surface and tropospheric temperature appear to be represented consistently in the datasets, we computed the mean meridional circulation flux and the stationary eddy flux for temperature at 60°N for the 700 hPa level. As the upper air reconstructions and GCM data were only available at monthly resolution, the transient eddy flux was computed only for the three reanalysis datasets. Figure 4a shows the mean meridional flux for all datasets on a seasonal (DJF) resolution. Differences between the datasets clearly emerge. Large variability between the individual members of the GCM datasets can also be seen. We find that the 20CRv2 and 20CRv2c timeseries are more consistent with the ERA20CM and largely on the upper-end of the CCC400 ensemble. ERA20C is on the low end of the CCC400 and outside the range of the ERA20CM ensemble for almost all years. Looking at the reconstruction it appears that the interannual variability is comparable to 20CRv2, however the overall magnitude is at the low end of the models, comparable to ERA20C until the 1930s. After that, the reconstruction agrees better with ERA20CM and the 20CR versions. Interestingly, mean meridional heat transport in the reconstruction during the ETCAW is rather low, with a strong drop around 1920. Finally, the ERA20C dataset shows the least interannual variability and has mean

values at the lower edge of the GCM ensembles. Looking at the evolution of this timeseries, it appears to be very stable throughout the century with no obvious trends. Since the 700 hPa temperatures in Fig. 3 seem to be consistent, we suspect that differences between datasets are mainly caused by different representations of meridional wind speed.

Figure 4b illustrates the stationary eddy flux for all gridded datasets. The seasonally averaged values show again the lower variability in ERA20C, with absolute values around the low range of the GCM ensembles. The reconstruction, 20CRv2 and 20CRv2c agree fairly well, especially so until 1940. These timeseries show a pronounced increase from 1900 until the 1930s, with a peak around 1930. This peak coincides very well with the circulation signal in the indices examined below (Fig. 7) and a few years after the reconstructed drop of the mean meridional

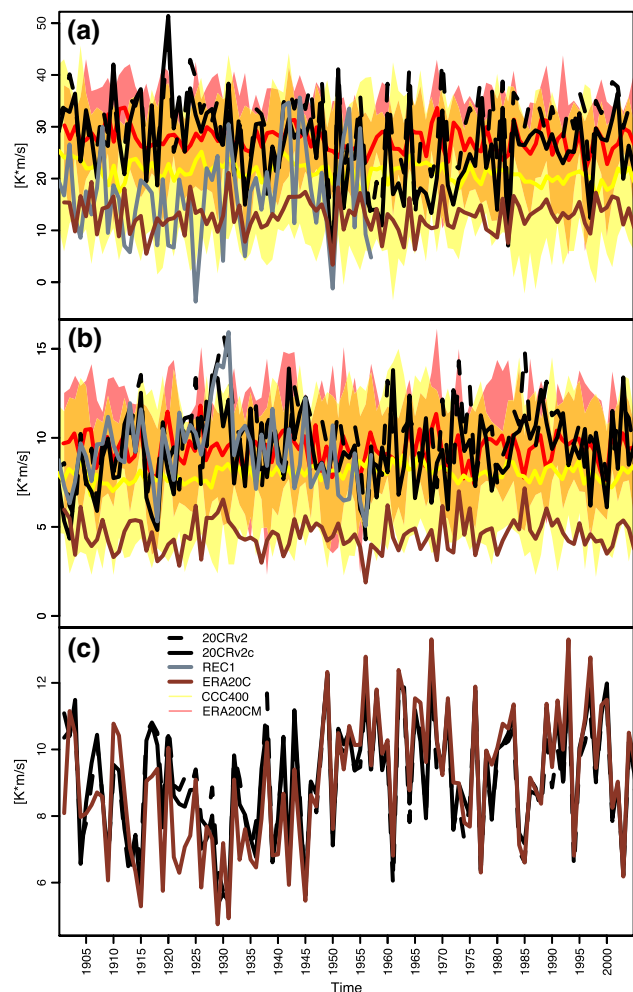


Fig. 4 **a** Mean meridional DJF heat flux at 60°N between 1900 and 2005 at 700 hPa for all gridded datasets, **b** the same for stationary heat flux and **c** the same for transient eddy heat flux, but only for reanalysis datasets (see also Supplementary Figure 6 for a sum of all three fluxes). Plotting conventions are as in Fig. 3

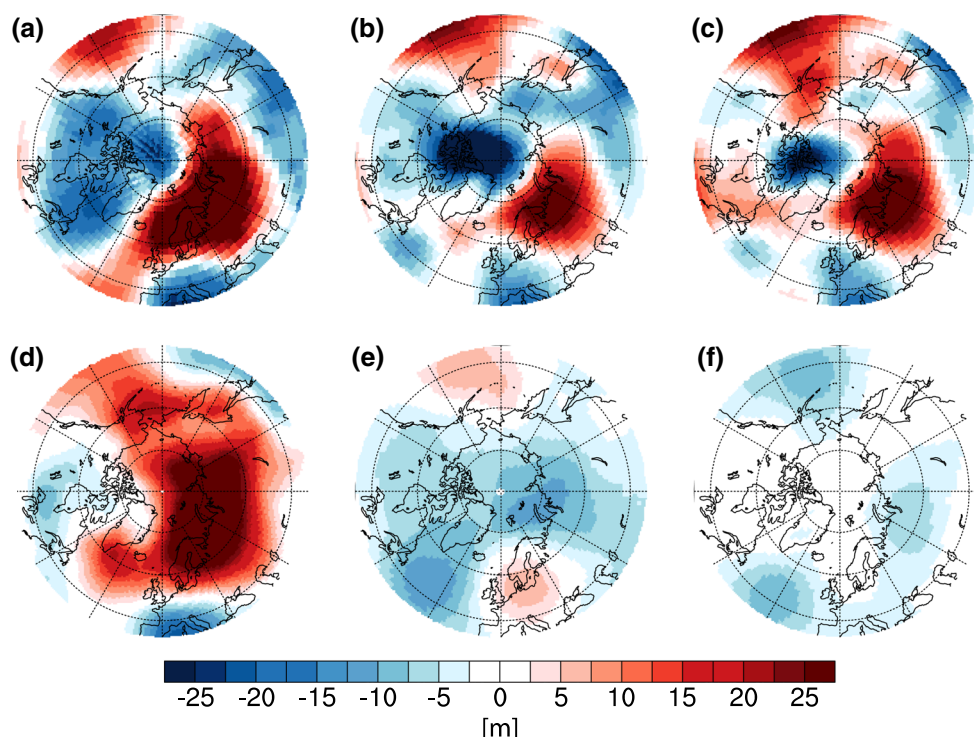


Fig. 5 Maps of time-averaged 700 hPa geopotential height anomalies for DJF 1920–1939 with respect to DJF 1971–2000 in **a** REC1 + ERA40, **b** 20CRv2, **c** 20CRv2c, **d** ERA20C, **e** ERA20CM ensemble mean, **f** CCC400 ensemble mean

circulation in Fig. 4a. However, this peak is reduced in magnitude in 20CRv2c. After 1940 all three datasets stay well within the GCM range. It is noteworthy that the ERA20C timeseries, although missing the absolute magnitude of fluxes, shares a highly significant 0.8 correlation with the 20CRv2 timeseries. Moreover, a peak period around 1930 is visible in ERA20C, but weaker than in 20CRv2. Since ERA20C shares the observational pressure input data with 20CRv2c, and uses the same assimilating model as the ERA20CM, the difference in magnitude is caused either by the different assimilation schemes or the assimilation of near-surface marine winds in ERA20C.

Depicting the transient eddy heat flux, Fig. 4c shows the evolution of the winter northward heat transport by weather systems such as cyclones and anticyclones in the three reanalysis products. Since monthly means were used as the base period for eddy transport, larger transient waves can also contribute to this transport term. However, a monthly base period ensured comparability. All three datasets show a strong interannual variability. However, compared to the mean meridional and stationary eddy flux, ERA20C shows a very good agreement in magnitude and variability with 20CRv2 and 20CRv2c, which only show minor deviations from one another, except for the 1920s. Moreover, in all three datasets the ETCAW decades show the lowest transient eddy flux values compared to the rest of the decades

during the twentieth century. Highest values can be found during the 1960s and the beginning of the 1970s, with a period of relatively stable increase between 1940 and 1970. Towards the end of the twentieth century, winter transient eddy heat flux at 700 hPa appears to decrease again.

4.3 Tropospheric stationary eddies

To investigate more into the striking inter-dataset differences in stationary eddy flux as well as the temporal evolution of the heat transport, we depict the ETCAW atmospheric circulation as seasonal mean geopotential height (GPH, Fig. 5) and temperature anomalies (Fig. 6) at 700 hPa during the period 1920–1939 for winter. Reanalysis and reconstruction datasets depict a strong positive geopotential height anomaly over the Eurasian part of the Arctic associated with negative or weaker anomalies over Greenland and the Canadian Archipelago (Fig. 5). This height distribution enhances meridional winds over the North Atlantic and transports southern airmasses into the Arctic domain. The ensemble mean anomalies of both GCMs show only weak signals, with a small positive signal over northern Europe in ERA20CM. CCC400 and ERA20CM show a comparable GPH anomaly pattern over the Atlantic and Eurasia, but disagree over the North Pacific domain. While an overall weaker signal is present in the

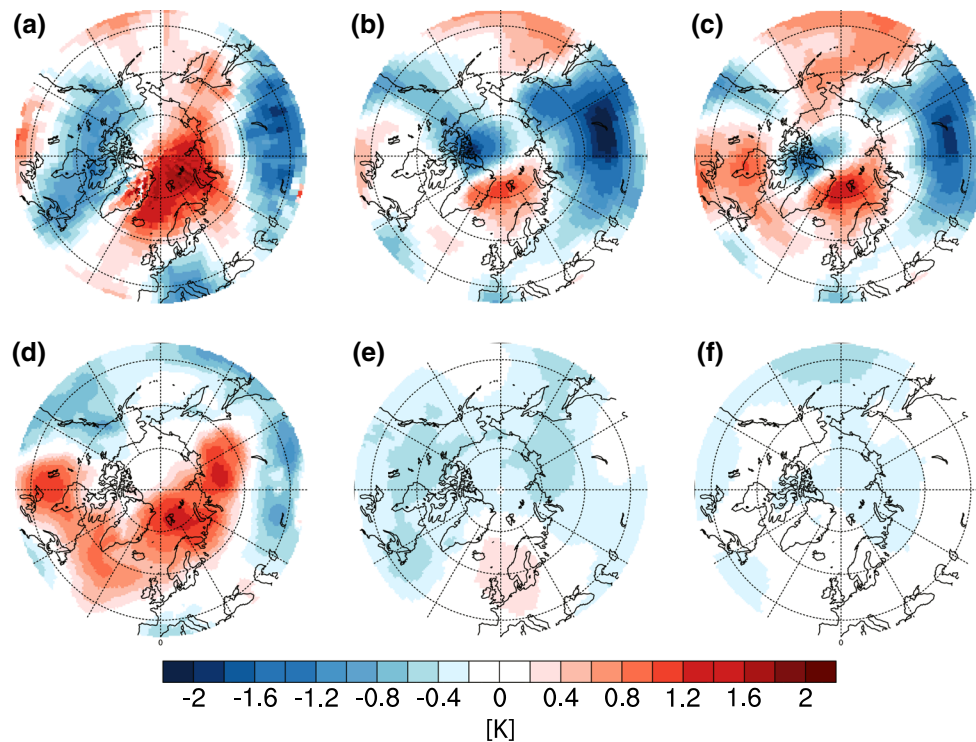


Fig. 6 Maps of time-averaged 700 hPa temperature anomalies for DJF 1920–1939 with respect to DJF 1971–2000 in **a** REC1 + ERA40, **b** 20CRv2, **c** 20CRv2c, **d** ERA20C, **e** ERA20CM ensemble mean, **f** CCC400 ensemble mean

ERA20CM ensemble mean over Europe, the pattern shows relative agreement with the reanalysis datasets, suggesting some forcing from either or both of the specified boundary conditions and radiative forcing. Both the GPH signal (Fig. 5d) and warming signal (Fig. 6d) are very prominent in the ERA20C dataset, with positive anomalies dominating nearly all of the Arctic domain, particularly for temperature (Fig. 6d). It is important to note that REC1 + ERA40 and 20CRv2 show a more heterogeneous anomaly structure and a more pronounced gradient between Europe and Canada. 20CRv2c emphasizes the Pacific positive anomaly, especially over Alaska, compared to 20CRv2. Over most of the hemisphere, positive GPH anomalies in 20CRv2c (Fig. 5c) tend to be increased compared to 20CRv2 (Fig. 5b), whereas the strength of central Arctic negative anomaly is reduced.

One result of the pressure anomalies is the noticeable warming at 700 hPa over the European sector of the Arctic. Positive North Pacific geopotential height and North American temperature anomalies seem to be placed much more northerly in the ERA20 datasets (Fig. 6). This is probably due to the known overestimation of Arctic sea level pressure, especially before 1950, in the ERA20C dataset (see Belleflamme et al. 2015). As with geopotential height, 20CRv2c amplifies the warming regions of 20CRv2 and decreases the magnitude of the Siberian negative anomaly.

This might be the result of reduced Arctic temperatures at the end of the twentieth century in 20CRv2c compared to 20CRv2 (Fig. 2). Generally, the strongest differences between all datasets appear over the Pacific sector, which is a result of the sparse observations for this region at the time of the ETCAW (Cram et al. 2015).

It is important to note that the GCM datasets mostly disagree with the observational datasets on the sign of the temperature signal (Fig. 6). This is due to the choice of reference period. The late decades of the twentieth century in the GCMs are mainly driven by the greenhouse gas and SST forcing which results in a relatively strong Arctic warming (e.g., Compo and Sardeshmukh 2009). If the reference period is changed to 1900 and 1919 (supplementary Figure 7) the warming signal is visible, with a second warming pole over the North Pacific. The same is true for the geopotential height anomalies (not shown). Thus a fraction of the circulation and associated temperature signal is forced.

To analyze the temporal evolution of this tropospheric pattern, we computed the GPH indices (Fig. 1) for DJF at 700 hPa geopotential height. We assume that during winter most of the heat influx into the Arctic originates from air-masses over the relatively mild oceans. Figure 7 shows the decadal averaged index (Eq. 2) values for each dataset on the 700 hPa level, for both the Atlantic and Pacific sector. As

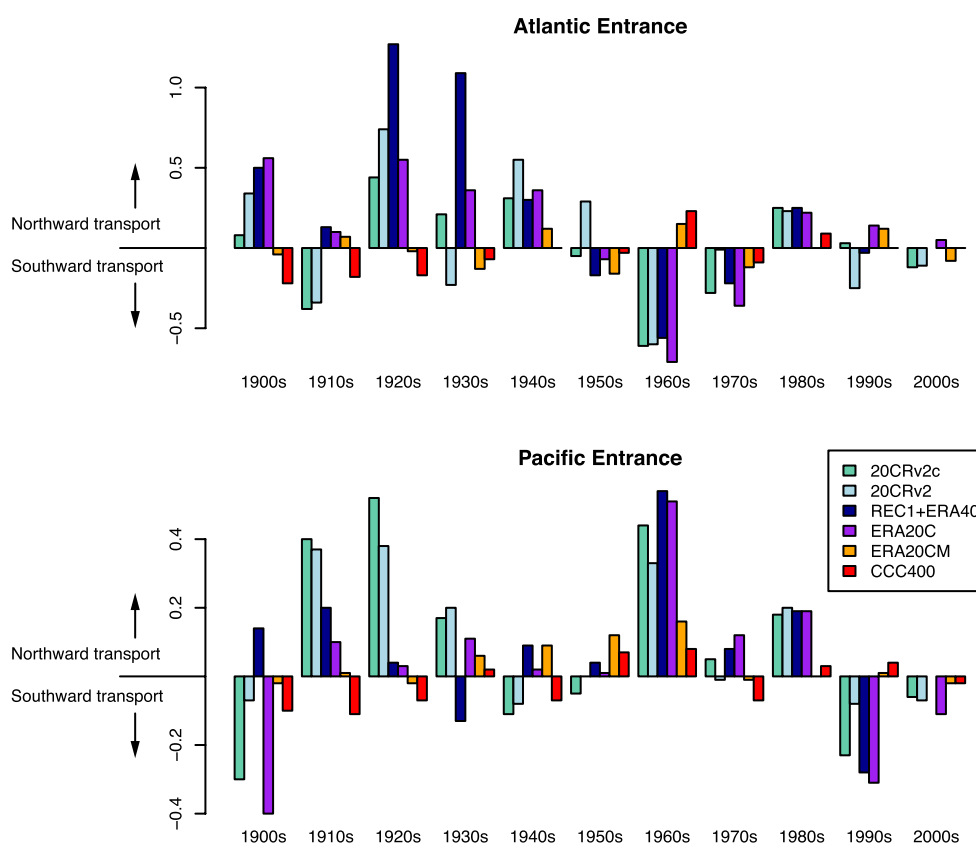


Fig. 7 700 hPa geopotential height circulation index values for (*top*) Atlantic sector (gradient 60° – 70° N 30° – 60° W Greenland to 60° – 70° N 60° – 100° E Siberia), (*bottom*) Pacific sector (gradient 60° – 70° N 150° – 180° W far east to 60° – 70° N 150° – 180° E Alaska). See Fig. 1 for regions

can be seen, reanalysis and reconstruction datasets show a peak in positive values between 1920 and 1940, especially for the 1920s where they show strong positive values. Both model datasets show much weaker gradients, also due to the ensemble mean computations. Moreover, during the ETCAW 1920s period both model datasets show an opposite sign of both indices. Both also show an opposite since for the Atlantic index in the 1930s (Fig. 7 top). Therefore, the enhanced northward circulation in both regions throughout the ETCAW is clearly captured by reanalyses and reconstructions, whereas the GCM datasets do not resolve this consistent signal. Interestingly, the recent warming does not coincide with a positive index, underlining the idea of a radiation-driven warming. Over the Atlantic sector in the 1920s, 20CRv2c shows a smaller geopotential height gradient, leading to reduced index values for the ETCAW. Nevertheless, the index is still positive, and 20CRv2c agrees well with the other observationally based datasets over time.

Looking at the Pacific sector, the index during the ETCAW period appears to be mostly positive as well, which supports a northward transport of maritime air-masses into the Arctic domain. Interestingly, 20CRv2c stands out with the highest Pacific index values during the

1920s of the ETCAW. Again, GCMs have difficulties to represent the index. It should be noted that the 1960s show an exceptionally strong northward airmass transport and dataset agreement in the Pacific sector, but more southward winds in the Atlantic sector.

These findings support the exceptional role of the circulation during the ETCAW. Especially the 1920s and 1930s show high peaks in the observational datasets, whereas the GCMs cannot reproduce this signal. Comparing the 2000s with the ETCAW, all datasets agree on a more southward circulation over the northern part of the oceans, hinting at a different Arctic warming mechanism [see Serreze and Barry (2011) for an overview], including possibly the hydrodynamic-radiative teleconnection suggested by Compo and Sardeshmukh (2009).

5 Discussion

The ETCAW is an exceptional feature in the climate evolution of the twentieth century and, as such, has been the subject of considerable previous analysis and discussion by the research community. Because of both location and

date of the warming, meteorological observations concerning the ETCAW are scarce and isolated. Here we used a variety of gridded atmospheric datasets: GCM simulations, reanalyses and reconstructions, to address some of the open questions regarding the ETCAW.

Our results support the findings of Wood and Overland (2010) who investigated the meridionalisation of circulation in the Arctic domain, including 20CRv2. We extended this idea to a new set of gridded datasets to gain more insight into the ultimate cause of the ETCAW. Surface and 700 hPa Temperatures in reanalysis datasets agree very well with reconstructed temperatures. All timeseries show a warming for DJF temperatures during the ETCAW. A strong temperature drop in the late 1940s showed by the reanalysis datasets seems to be overestimated by the assimilation of only surface data. If upper air information is added, this drop is reduced.

Spatial anomalies with respect to 1971–2000 accentuated the differences between datasets. ERA20C displays the largest extent of positive anomalies, both in geopotential height and temperature. We suggest that this is probably due to an overestimation of Arctic SLP, especially before 1950 (Belleflamme et al. 2015). 20CRv2, 20CRv2c and REC1 + ERA40 are more heterogeneous with a distinct signal of positive anomalies over the European Arctic. GCM ensemble means lack most of these features (such as the strong temperature anomaly gradient from North America, to Europe), suggesting that most of the anomalies are not forced. Additionally, we found that individual GCM members have similar anomaly conditions in 700 hPa geopotential height and temperature (not shown), which underlines the impact of internal variability.

This analysis showed that prescribed SST and sea ice conditions, which are similar in the GCM and reanalysis datasets (except 20CRv2c), are not enough to produce the ETCAW spatial pattern. In fact these boundary conditions only lead to a spatially averaged warming (as can be seen in the 700 hPa temperature timeseries). Furthermore, when comparing ERA20CM to ERA20C, which share model architecture, specified radiative constituents, and have similar boundary conditions, it becomes obvious that assimilation of observations is needed to produce the distinct spatial patterns of the ETCAW.

The elevated temperatures in the GCMs during the ETCAW suggest that this event is not completely independent of the SSTs. Dependent on the timescales, elevated SSTs could trigger a change in the circulation patterns directly as well as an increase in advected heat without a change in the circulation through an increase in the temperature part of the advection equation. However, we found that the atmospheric circulation variability is the most important factor generating the ETCAW signal since the GCMs could not reproduce the main features of the

reanalysis or reconstructions. Therefore, our results suggest that atmospheric intrinsic variability played a major role in the formation of the ETCAW. This supports the findings of Wood and Overland (2010) as well as Beitsch et al. (2014), who underline the atmospheric internal variability part of the ETCAW.

Based on the anomaly patterns, indices were defined to analyze the evolution of this circulation condition over time. Our results suggest a meridional circulation pattern during the ETCAW that supported maritime southerly winds over both the Atlantic and Pacific part of the Arctic. We found this to be a rather exceptional Arctic circulation condition with respect to the twentieth century. The only decade that shows a similar circulation is the 1980s, however the signal is much weaker in amplitude. For the current warming period (2000–2009), no such signal is found. It is noteworthy that both GCMs were not able to mirror this evolution throughout the century. Concerning the influence of more zonal indices like the North Atlantic Oscillation (NAO), Arctic Oscillation (AO) or the Pacific—North American Index (PNA), Wood and Overland (2010) found that in the second half of the twentieth century, after the ETCAW, AO and PNA combined can explain 44 % of the Arctic SAT variability. However with the beginning of the SAT increase ca. 1920, meridional indices take over and display high values up until ca. 1950. Therefore, our findings of increased meridionalisation over the Atlantic support the results of earlier studies (Scherhag 1939; Grant et al. 2009; Wood and Overland 2010).

Moreover, our findings agree very well with the superposed epoch analysis of 26 ETCAW-like events of Beitsch et al. (2014). We could show that the mechanisms which governed the composite of the 26 modelled events in the study of Beitsch et al. (2014) also played an important role in the actual ETCAW. Among those mechanisms, we find an increase of stationary heat transport at 700 hPa (Fig. 4b) at the timing of the warming in the REC1 and 20CRv2 datasets. This peak also is consistent with the increased index values in the 1920s decade (Fig. 7) over the Atlantic and Pacific domain. The ERA20C dataset does not show an exceptional peak but rather has a period of prolonged high values (relative to this dataset's long-term average) and an overall highly significant correlation with 20CRv2 and a significant but smaller correlation with 20CRv2c (for correlation coefficients see supplement Tables 1–5). These findings suggest and underline that the ETCAW was the result of unusual internal variability. Moreover, our study points to the critical role of the Pacific (as did Overland et al. 2012 for the recent warming period), which should be investigated in more detail in the future. Since this is an atmosphere-only analysis, we cannot verify the ocean mechanisms proposed by Beitsch et al. (2014). Additionally, we found that the ensemble mean of the 30 and 10 member GCMs could not

resolve the dynamics needed for the spike (drop) in stationary heat transport (mean meridional transport).

As Beitsch et al. (2014) found in their model analysis, we find a decrease of mean meridional heat flux at 700 hPa right before the warming in the independent (no sea-surface temperatures are used) upper-air reconstruction. Finally, we investigated transient eddy fluxes at 700 hPa in the reanalysis datasets. In this case ERA20C agrees very well with 20CRv2 and 20CRv2c. Since the computation is based on a deviation from the monthly mean, it appears that the temperature monthly mean in ERA20C is probably overestimated during the ETCAW, but the daily variability agrees with other two data sets. The 1920s and 1930s together show the lowest decadal values of transient eddy heat flux during the whole twentieth century. This is true for all three reanalysis products examined.

Summarizing the findings for heat fluxes at 700 hPa, we found a reduction in mean meridional flux before the actual warming and an increase during the warming in the reconstructions. However, reanalyzed values for this metric might be unreliable, as suggested by the discrepancies in surface wind errors (see supplementary Figure 8) in all three reanalysis datasets [see also Swart et al. (2015) for similar issues in the Southern Hemisphere]. Additionally, we found an increase of stationary heat flux in reconstructions and reanalyses simultaneous with the ETCAW. Finally, all reanalysis products show a reduction of the transient eddy flux during the ETCAW.

Concerning the peculiarity of the ETCAW, the question arises if just many random events occurred between 1920 and 1939 or if there was actually a state change, either natural or forced, during that time. Considering external factors that could influence a warming, ENSO or volcanic eruptions (e.g., winter warming) would have the biggest impacts. However, no major explosive volcanic eruption occurred during that time. El Niño events occurred during 1918 (Giese et al. 2010) and 1942, with weaker conditions probably before and after these dates. Brönnimann et al. (2004) found a detectable impact on European climate for the 1939–1942 El Niño event, which temporarily interrupted the ETCAW period (Fig. 2). Nevertheless, Grant et al. (2009) found a remarkable jump of temperatures right at the start of the ETCAW after which temperatures plateaued at a high level. The initial trigger for this strong jump is still uncertain, but so far there are no signs for an exceptional variance increase (in temperature and stationary eddy flux) for the whole ETCAW period (see Supplement Table 6).

In the flux timeseries analyzed, the ETCAW and the current ongoing warming are appreciably different. No noticeable increase (decrease) of stationary (transient) eddy heat flux is shown for the end of the twentieth century, although a warming is clearly visible from the

temperature timeseries. Therefore, our findings suggest that the ETCAW was indeed governed by an exceptional case of internal atmospheric variability, rather than by changes in the Arctic radiative forcing.

6 Conclusion

An extensive set of simulated and observational gridded datasets was analyzed to examine the atmospheric conditions and their role during the ETCAW. Evidence was found for a major contribution of atmospheric internal climate variability in the spatial extent and structure of the warming. Utilizing the 700 hPa heat transport as a surrogate for tropospheric processes, it could be shown that reanalysis and reconstruction datasets have peak values of stationary heat flux during the ETCAW. We also found that the independent reconstruction shows a decrease of mean meridional heat flux prior to the warming and the analysis of reanalysis datasets exhibits a decrease of transient eddy heat flux into the Arctic domain. These results support theoretical modelling studies and demonstrate this behaviour for the first time in observational datasets.

Furthermore, by comparing GCM and reanalysis datasets, which share similar forcings, we have shown that the specified SST, sea ice, and radiative forcings are not sufficient to trigger the spatial pattern of the ETCAW. Instead, observational input is needed to compute the realistic circulation and associated heat flux response. Thus it can be concluded that the intrinsic atmospheric variability, rather than forcing, played a major part in the formation of the ETCAW signal. These findings are consistent with several previous studies. They highlight the importance of understanding the influence of internal variability in the context of climate change, especially in the Arctic region. Future projections of Arctic warming scenarios have to take into account the likelihood of such internal dynamics. The question remains open as to the precise trigger of the formation of the ETCAW circulation pattern and how different flux evolutions are linked to each other. Future studies may take advantage of newly digitized data with increased resolution. Coupled ocean-atmosphere datasets may need to be utilized for this purpose.

Acknowledgments The authors acknowledge funding by the European ERAnet.RUS programme, within the project ACPA, and by the European FP7 projects ERA-CLIM and ERA-CLIM2. Support for the Twentieth Century Reanalysis Project version 2c dataset is provided by the US Department of Energy, Office of Science Biological and Environmental Research (BER), and by the National Oceanic and Atmospheric Administration Climate Program Office. Support for the Twentieth Century Reanalysis Project dataset is provided by the US Department of Energy, Office of Science Innovative and Novel Computational Impact on Theory and Experiment (DOE INCITE)

program, and Office of Biological and Environmental Research (BER), and by the National Oceanic and Atmospheric Administration Climate Program Office.

References

- Pages 2K Consortium (2013) Continental-scale temperature variability during the past two millennia. *Nat Geosci* 6:339–346
- Beitsch A, Jungclauss JH, Zanchettin D (2014) Patterns of decadal-scale Arctic warming events in simulated climate. *Clim Dyn* 43:1773–1789
- Bekryaev RV, Polyakov IV, Alexeev VA (2010) Role of polar amplification in long-term surface air temperature variations and modern Arctic warming. *J Clim* 23:3888–3906
- Belleflamme A, Fettweis X, Erpicum M (2015) Recent summer Arctic atmospheric circulation anomalies in a historical perspective. *Cryosphere* 9:53–64
- Bengtsson L, Semenov VA, Johannessen OM (2004) The early twentieth-century warming in the Arctic—a possible mechanism. *J Clim* 17:4045–4057
- Bhend J, Franke J, Folini D, Wild M, Brönnimann S (2012) An ensemble-based approach to climate reconstructions. *Clim Past* 8:963–976
- Bindoff NL, Stott PA, AchutaRao M, Allen MR, Gillett N, Gutzler D, Hansingo K, Hegerl G, Hu Y, Jain S et al. (2013) Detection and attribution of climate change: from global to regional. Cambridge University Press, Cambridge, United Kingdom and New York, NY, USA
- Birkeland B (1930) Temperaturvariationen auf Spitzbergen. *Meteorol Z* 47:2
- Brohan P, Kennedy JJ, Harris I, Tett SFB, Jones PD (2006) Uncertainty estimates in regional and global observed temperature changes: a new data set from 1850. *J Geophys Res Atmos* 111:D12106
- Brönnimann S (2009) Early twentieth-century warming. *Nat Geosci* 2:735–736
- Brönnimann S, Luterbacher J, Staehelin J, Svendby TM, Hansen G, Svenøe T (2004) Extreme climate of the global troposphere and stratosphere in 1940–42 related to El Niño. *Nature* 431:971–974
- Brönnimann S, Grant AN, Compo GP, Ewen T, Griesser T, Fischer AM, Schraner M, Stickler A (2012) A multi-data set comparison of the vertical structure of temperature variability and change over the Arctic during the past 100 years. *Clim Dyn* 39:1577–1598
- Compo GP, Sardeshmukh PD (2009) Oceanic influences on recent continental warming. *Clim Dyn* 32:333–342. doi:10.1007/s00382-008-0448-9
- Compo GP, Whitaker JS, Sardeshmukh PD, Matsui N, Allan RJ, Yin X, Gleason BE, Vose RS, Rutledge G, Bessemoulin P (2011) The Twentieth Century Reanalysis project. *Q J R Meteorol Soc* 137:1–28. doi:10.1002/qj.776
- Cram TA, Compo GP, Yin X, Allan RJ, McColl C, Vose RS, Whitaker JS, Matsui N, Ashcroft L, Auchmann R et al (2015) The international surface pressure databank version 2. *Geosci Data* 2:31–46
- Crowley TJ, Zielinski G, Vinther B, Udisti R, Kreutz K, Cole-Dai J, Castellano E (2008) Volcanism and the little ice age. *PAGES News* 16:22–23
- Delworth TL, Knutson TR (2000) Simulation of early 20th century global warming. *Science* 287:2246–2250
- Fyfe JC, von Salzen K, Gillett NP, Arora VK, Flato GM, McConnell JR (2013) One hundred years of Arctic surface temperature variation due to anthropogenic influence. *Nat Sci Rep* 3:2645
- Giese BS, Compo GP, Slowey NC, Sardeshmukh PD, Carton JA, Ray S, Whitaker JS (2010) The 1918/1919 El Niño. *Bull Am Meteorol Soc* 91:177–183. doi:10.1175/2009BAMS2903.1
- Giese BS, Seidel HF, Compo GP, Sardeshmukh PD (2016) An ensemble of historical ocean reanalyses with sparse observational input. *J Geophys Res Oceans* (submitted)
- Grant A, Brönnimann S, Haimberger L (2008) Recent arctic warming vertical structure contested. *Nature* 455:E2–E3
- Grant AN, Brönnimann S, Ewen T, Griesser T, Stickler A (2009) The early twentieth century warm period in the European Arctic. *Meteorol Z* 18:425–432
- Griesser T, Brönnimann S, Grant A, Ewen T, Stickler A, Comeaux J (2010) Reconstruction of global monthly upper-level temperature and geopotential height fields back to 1880. *J Clim* 23:5590–5609
- Hansen J, Ruedy R, Sato M, Lo K (2010) Global surface temperature change. *Rev Geophys* 48:RG4004
- Hanssen-Bauer I, Førland EJ (1998) Long-term trends in precipitation and temperature in the Norwegian Arctic: can they be explained by changes in atmospheric circulation patterns? *Clim Res* 10:143–153
- Hersbach H, Peubey C, Simmons A, Berrisford P, Poli P, Dee D (2015) ERA-20CM: a twentieth-century atmospheric model ensemble. *Q J R Meteorol Soc* 141:2350–2375
- Hirahara S, Ishii M, Fukuda Y (2014) Centennial-scale sea surface temperature analysis and its uncertainty. *J Clim* 27:57–75
- IPCC (2013) Climate Change 2013: the physical science basis. In: Stocker TF, Qin D, Plattner G-K, Tignor M, Allen SK, Boschung J, Nauels A, Xia Y, Bex V, Midgley PM (eds) Contribution of working group I to the fifth assessment report of the intergovernmental panel on climate change. Cambridge University Press, Cambridge, p 1535
- Johannessen OM, Bengtsson L, Miles MW, Kuzmina SI, Semenov VA, Alekseev GV, Nagurnyi AP, Zakharov VF, Bobylev LP, Pettersson LH (2004) Arctic climate change: observed and modelled temperature and seaice variability. *Tellus A* 56:328–341
- Jungclauss JH, Lorenz SJ, Timmreck C, Reick CH, Brovkin V, Six K, Segschneider J, Giorgetta MA, Crowley TJ, Pongratz J (2010) Climate and carbon-cycle variability over the last millennium. *Clim Past* 6:723–737
- Kaufman DS, Schneider DP, McKay NP, Ammann CM, Bradley RS, Briffa KR, Miller GH, Otto-Bliessner BL, Overpeck JT, Vinther BM (2009) Recent warming reverses long-term Arctic cooling. *Science* 325:1236–1239
- Koch D, Jacob D, Tegen I, Rind D, Chin M (1999) Tropospheric sulfur simulation and sulfate direct radiative forcing in the Goddard Institute for Space Studies general circulation model. *J Geophys Res Atmos* 104:23799–23822
- Lean J (2000) Evolution of the Sun's spectral irradiance since the Maunder Minimum. *Geophys Res Lett* 27:2425–2428
- Mann ME, Woodruff JD, Donnelly JP, Zhang Z (2009) Atlantic hurricanes and climate over the past 1,500 years. *Nature* 460:880–883
- Opel T, Fritzsche D, Meyer H (2013) Eurasian Arctic climate over the past millennium as recorded in the Akademii Nauk ice core (Severnaya Zemlya). *Clim Past* 9:2379–2389
- Overland JE, Turet P (1994) Variability of the atmospheric energy flux across 70 N computed from the GFDL data set. In: Johannessen OM, Muench RD, Overland JE (eds) The polar Oceans and their role in shaping the global environment. American Geophysical Union, Washington, pp 313–325
- Overland JE, Francis JA, Hanna E, Wang M (2012) The recent shift in early summer Arctic atmospheric circulation. *Geophys Res Lett* 39:L19804
- Overpeck J, Hughen K, Hardy D, Bradley R, Case R, Douglas M, Finney B, Gajewski K, Jacoby G, Jennings A (1997)

- Arctic environmental change of the last four centuries. *Science* 278:1251–1256
- Poli P, Hersbach H, Dee DP, Berrisford P, Simmons AJ, Vitart F, Laloyaux P, Tan DGH, Peubey C, Thépaut J-N, Trémolet Y, Hólm EV, Bonavita M, Isaksen I, Fisher M (2016) ERA-20C: an atmospheric reanalysis of the 20th century. *J Clim*. doi:10.1175/JCLI-D-15-0556.1
- Polyakov IV, Bekryaev RV, Alekseev GV, Bhatt US, Colony RL, Johnson MA, Maskshas AP, Walsh D (2003) Variability and trends of air temperature and pressure in the maritime Arctic, 1875–2000. *J Clim* 16:2067–2077
- Pongratz J, Reick C, Raddatz T, Claussen M (2008) A reconstruction of global agricultural areas and land cover for the last millennium. *Glob Biogeochem Cycles* 22:GB3018
- Rayner NA, Parker DE, Horton EB, Folland CK, Alexander LV, Rowell DP, Kent EC, Kaplan A (2003) Global analyses of sea surface temperature, sea ice, and night marine air temperature since the late nineteenth century. *J Geophys Res Atmos* 108:4407
- Roeckner E, Brokopf R, Esch M, Giorgetta M, Hagemann S, Kornbluh L, Manzini E, Schlese U, Schulzweida U (2006) Sensitivity of simulated climate to horizontal and vertical resolution in the ECHAM5 atmosphere model. *J Clim* 19:3771–3791
- Scherhag R (1939) Die Erwärmung des Polargebiets. *Annalen der Hydrographie* 67:57–67
- Schlesinger ME, Ramankutty N (1994) An oscillation in the global climate system of period 65–70 years. *Nature* 367:723–726
- Semenov V, Latif M (2012) The early twentieth century warming and winter Arctic sea ice. *Cryosphere* 6:1231–1237
- Serreze MC, Barry RG (2011) Processes and impacts of Arctic amplification: a research synthesis. *Glob Planet Change* 77:85–96
- Swart NC, Fyfe JC, Gillett N, Marshall GJ (2015) Comparing trends in the southern annular mode and surface westerly jet. *J Clim* 28:8840–8859
- Thompson DM, Cole JE, Shen GT, Tudhope AW, Meehl GA (2015) Early twentieth-century warming linked to tropical Pacific wind strength. *Nat Geosci* 8:117–121
- Uppala SM, Kållberg PW, Simmons AJ, Andrae U, Bechtold V, Fiorino M, Gibson JK, Haseler J, Hernandez A, Kelly GA (2005) The ERA-40 reanalysis. *Q J R Meteorol Soc* 131:2961–3012
- Wagner A (1940) *Klimaänderungen und Klimaschwankungen*. Vieweg + Teubner Verlag, Braunschweig
- Wegmann M, Brönnimann S, Bhend J, Franke J, Folini D, Wild M, Luterbacher J (2014) Volcanic influence on European summer precipitation through monsoons: possible cause for “Years without Summer”? *J Clim* 27:3683–3691
- Wood KR, Overland JE (2010) Early 20th century Arctic warming in retrospect. *Int J Climatol* 30:1269–1279
- Wood KR, Overland JE, Jónsson T, Smoliak BV (2010) Air temperature variations on the Atlantic-Arctic boundary since 1802. *Geophys Res Lett* 37:L17708
- Yoshimori M, Raible CC, Stocker TF, Renold M (2010) Simulated decadal oscillations of the Atlantic meridional overturning circulation in a cold climate state. *Clim Dyn* 34:101–121